Volume 142, Number 8, 2007 ISSN 0038-1098
published 20 May 2007

ELSEVIER

solid state communications

an international journal

Containing a Fast-track Communication

Available online at ScienceDirect
www.sciencedirect.com

www.elsevier.com/locate/ssc

Available online at www.sciencedirect.com
ScienceDirect
Solid State Communications 142 (2007) 441–444
solid state communications
www.elsevier.com/locate/ssc

SnO_2/In_2O_3 one-dimensional nano-core–shell structures: Synthesis, characterization and photoluminescence properties

Y. Li*, G. Xu, Y.L. Zhu, X.L. Ma, H.M. Cheng

Shenyang National Laboratory for Materials Science, Institute of Metal Research, Chinese Academy of Sciences, Shenyang 110016, PR China

Received 28 July 2006; accepted 21 March 2007 by B.-F. Zhu
Available online 28 March 2007

Abstract

SnO_2/In_2O_3 one-dimensional nano-core–shell structures have been synthesized at 1350 °C by thermal evaporation of the mixture of metal Sn, $Fe(NO_3)_3$ powders and In particles. The as-synthesized products have been characterized by energy-dispersive X-ray spectroscopy, selected-area electron diffraction and high-resolution transmission electron microscopy. Microstructure characterization indicates the orientation relationship between core and shell is $[001]_{In_2O_3} \parallel [001]_{SnO_2}$, $(010)_{In_2O_3} \parallel (010)_{SnO_2}$. The formation mechanism of this nano-core–shell structure can be attributed to the cover of In_2O_3 on the surface of SnO_2 nanochains. The photoluminescence properties of the nano-core–shell structures have been measured. The PL spectrum shows some difference with the result from pure SnO_2 and In_2O_3 nanostructure that be deemed to relate to interface defects in SnO_2/In_2O_3 nano-core–shell structure.

PACS: 68.37.Lp; 61.82.Fk; 78.55.-m

Keywords: A. Semiconductors; B. Nanofabrications; C. Scanning and transmission electron microscopy; D. Optical properties

1. Introduction

Recently, compound semiconductor one-dimensional (1D) nanostructures have attracted significant research interest, due to their important application potential as building blocks of nanoscale electronic or optoelectronic devices exploiting their properties not achievable in bulk states [1–3]. Among all the 1D nanostructures, 1D nano-core–shell structures (or named nanocables) have more extensive application in field emitter devices, electronic transport and other electrical devices, because of their distinct double layer structure and interaction of double layer. The first 1D nano-core–shell structures are silicon carbide and silicon oxide sheathed with boron nitride and carbon that was synthesized by means of reactive laser ablation in 1998 [4], in succession, a series of metal–metal, metal–metal oxide and metal oxide–metal oxide 1D nano-core–shell structures successfully synthesized by thermal evaporation, chemical vapour deposition, coelectrodeposition and epitaxial synthesis method [5–11].

In particular, as wide band gap semiconductor (direct band gap energy of 3.6 eV), IIIB, IVB group oxide SnO_2 and In_2O_3 1D nanostructures are more attractive because they are candidates for fabricating electronic and optoelectronic nanodevices [12–14]. Therefore, various SnO_2 and In_2O_3 1D nanostructure have been synthesized successively via different preparation methods [15–18]. However, to our knowledge, preparation and study of SnO_2/In_2O_3 1D nano-core–shell structures have not been reported up to now.

In this paper, we report the successful synthesis of SnO_2/In_2O_3 1D nano-core–shell structures by thermal evaporation of the powders of metal Sn, $Fe(NO_3)_3$ and In particles. The as-synthesized products have been characterized by energy-dispersive X-ray spectroscopy (EDX), selected-area electron diffraction (SAED) and high-resolution transmission electron microscopy (HREM). The photoluminescence (PL) properties of the as-synthesized products have also been measured. On the basis of investigation of the microstructures, the possible formation mechanism of SnO_2/In_2O_3 1D nano-core–shell structures and the potential relation

* Corresponding address: Shenyang National Laboratory for Materials Science, Institute of Metal Research, Chinese Academy of Sciences, Wenhua Road 72, Shenyang 110016, PR China. Fax: +86 24 23971215.
E-mail address: yingli@imr.ac.cn (Y. Li).

0038-1098/$ - see front matter
doi:10.1016/j.ssc.2007.03.031

between microstructure and photoluminescence properties were discussed.

2. Experimental

A horizontal alumina tube was mounted inside a tubular furnace. Powders of metal tin (3 g, 99.0%), $Fe(NO_3)_3 9H_2O$ (20 g), and indium particles (3 g, 99%), were mixed and then placed in an alumina crucible. After transferring the crucible to the center of the alumina tube, the tube was evacuated by a mechanical rotary pump to pressure of 10 Pa. During the experiment, a constant flow of Ar mixed with 5% H_2 was maintained at a flow rate of 50 sccm (standard cubic centimetres per minute) and the pump continually evacuated the system so that the pressure inside the tube was kept at 2×10^4 Pa. The temperature of alumina tube was increased from room temperature to 1350 °C and held at this temperature for 100 min. After the furnace was cooled down to room temperature, grayish cotton-like products were found on the top of inner wall of tube. Low-magnification images and selected-area electron diffraction of the as-deposited products were taken on a JEOL-2010 transmission electron microscope. Tecnai G^2 F30 transmission electron microscope, equipped with high-angle-angular-dark-field (HAADF) detector, Gatan imaging-filter (GIF) and energy X-ray dispersive spectroscopy (EDX) systems, was used for Z-contrast imaging and composition line analysis. Room-temperature PL spectrum was measured on a Hitachi F-4500 fluorescence spectrophotometer equipped with a Xe lamp.

3. Results and discussion

Fig. 1(a) is a TEM image clearly showing the typical morphology of the as-synthesized products. The products are mainly constituted of 1D nano-core–shell structures, among which representative one was marked by a black arrow. A small amount of nanobelts and nanowires were also observed. It is seen that the diameters of these 1D nano-core–shell structures are about several hundred nanometers and the lengths range from several micrometres to several-hundred micrometres. Fig. 1(b) is a low magnification HAADF image of one of the nano-core–shell structures. It can be clearly found that many rhombi-like structures kinked and grew to constitute the cores. To verify the composition of the shells and the cores, the EDX point and line scanning have been performed from the point and the line in Fig. 1(b). As shown in Fig. 1(c), the point scanning result reveals that the nano-core–shell structures are constituted of In, Sn, and O element where the Cu and C are from microgrid and carbon film used to support the 1D structures. Fig. 1(d) is the EDX line-scanning result that can give a detailed analysis of composition fluctuation across the diameter of the 1D structure. It is seen that a clear heave of Sn and descent of In occurs in part of the core. But the fact that the middle of the 1D nano-core–shell structure does not have the least In content may imply the existence o some indium element in the core. The fluctuating result of the oxygen element is not given here for its change is unclear.

Fig. 2(a) is a low-magnification TEM image of a nano-core–shell structure showing clearly core-shell structure and

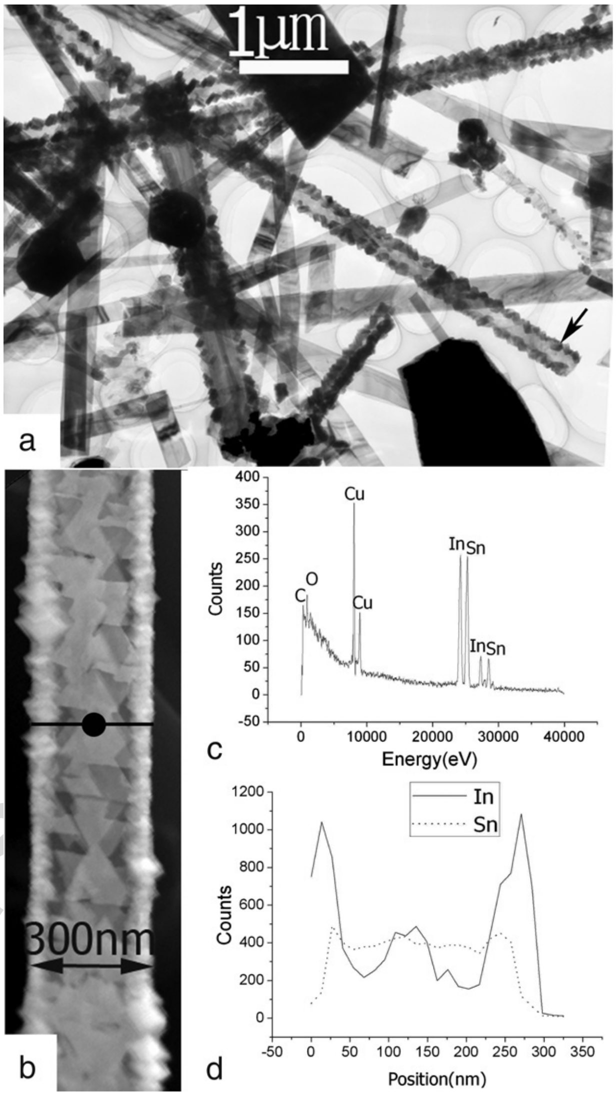

Fig. 1. (a) A TEM image shows the typical morphologies of the as-synthesized products, (b) A low magnification HAADF image of one of the SnO_2/In_2O_3 1D nano-core–shell structures, (c) and (d) EDX analysis results corresponding to the point scanning and line scanning across the 1D nano-core–shell structure in (b).

rhombi-like cores. The sharp angle of the rhombi is about 77° that marked in a rhombus. In addition, some ledges marked by arrows were found on the two sides of the nano-core–shell structure. Fig. 2(b) is the corresponding SAED pattern from the nano-core–shell structure in (a). The SAED pattern can be indexed as In_2O_3 with a body centred cubic structure and SnO_2 with orthorhombic structure, their lattice constant is $a = 10.05$ Å for In_2O_3 and $a = 4.72$ Å, $b = 5.73$ Å, $c = 5.21$ Å for SnO_2. They agree well with the reported values from JPCDS card (76-0152) and (29-1484). The characteristic diffraction spots of SnO_2 and In_2O_3 were signed with subscript '*S*' and '*I*', respectively. This SAED pattern was gained with incident beam parallel to [001] direction of In_2O_3 and SnO_2, in which the orientation relationship is given as $[001]_{In_2O_3} \parallel [001]_{SnO_2}$, $(010)_{In_2O_3} \parallel (010)_{SnO_2}$. The growth direction of the In_2O_3 shell and SnO_2 cores are same along the [010] lattice direction. Because of their near plane distance, the (100) diffraction spots

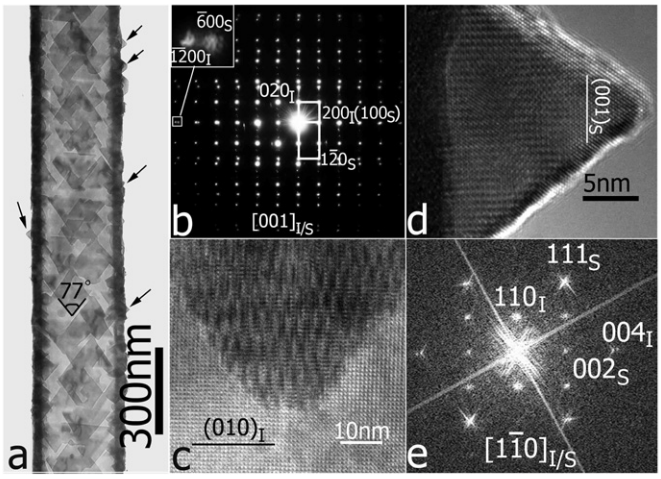

Fig. 2. (a) A low-magnification TEM image showing general characteristics of microstructures in the as-synthesized 1D nano-core–shell structures (b) the corresponding SAED pattern from the nano-core–shell structure in (a). (c) HREM image from the area marked in (a). (d) The HREM image corresponding to one of the ledges marked by arrows. (e) The FT pattern of the HREM image in (d).

plane of SnO_2 is overlapped with the (200) diffraction spots of In_2O_3. Their diffraction spots along [100] direction can be distinguished at high-index spots, for example, the inserted partial magnified image shows the $(\bar{6}00)$ diffraction spot of SnO_2 is easily distinguished from the $(\overline{12}00)$ diffraction of In_2O_3. In contrast to that, the (010) plane distance of SnO_2 is much bigger than that of the (020) from In_2O_3, the diffraction spot is split obviously. The results of HREM in Fig. 2(c) further verified this conclusion of SAED results, in which the characteristic lattice image of In_2O_3 is signed. Fig. 2(c) also shows a corner of the rhombi-like cores, the morie pattern comes from the overlapping of SnO_2 cores and In_2O_3 shell. The characteristic ledge also was magnified in Fig. 2(d), and the corresponding Fourier Transformation (FT) pattern was given in Fig. 2(e). Obviously, the tip of ledges is SnO_2 while the bottom is a mixture of SnO_2 and In_2O_3. The FT pattern shows the growth direction of the ledge is [001] lattice direction of In_2O_3.

As to formation mechanism of these 1D nano-core–shell structures, a possible schematic illustration was provided in Fig. 3. It is well-known that $Fe(NO_3)_3$ decomposes stepwise Fe_2O_3, NO_2, and O_2 at temperature higher than 125 °C. The melting point of metal indium and tin are relative lower, at 430 K, 505 K, respectively. When the temperature reaches a critical value, the two metals start to melt, the melted quantity of indium being less than that of tin since the surface to volume ratio of indium particles is much smaller than that of tin powders. The melting metal tin will react with the oxygen and yield tin oxide. A little of the melting indium may be enclosed by tin. As the {110} planes are relative closed packed with orthorhombic tin oxide, the rhombi constituting SnO_2 {110} lattice plane were formed. It is the reason that the angle of the rhombi in Fig. 2(a) is about 77°, which is approximately equal to the angle 78.9° between lattice plane (110) and $(1\bar{1}0)$. A few indium elements in the formed rhombi may act as a catalyst. When the SnO_2 rhombi with a little of indium and indium

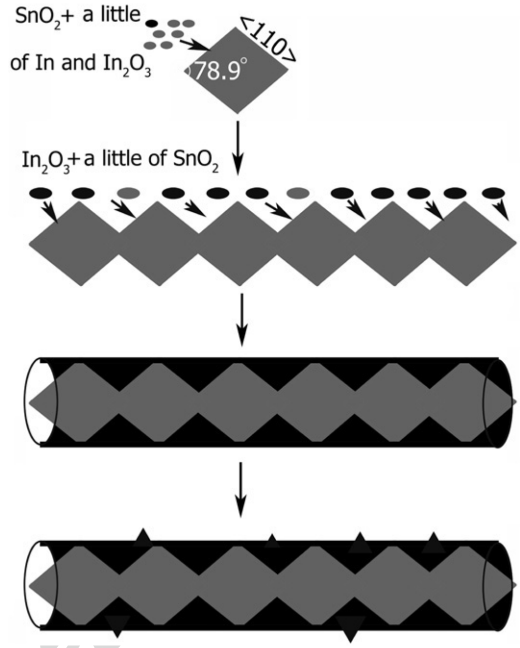

Fig. 3. Schematic illustration showing the possible growth process of SnO_2/In_2O_3 1D nano-core–shell structures.

oxide are formed, many SnO_2 rhombi start to link and form a chain. Then, the In_2O_3 formed and adhered to the surface of SnO_2 chains, because the metal indium start to melt in large quantity with raise of the temperature, so the 1D nano-core–shell structure formed. Later, durative evaporation of two sorts of metal, react with oxygen will formed the ledge in the tube wall. Because of uncontrollable detailed react condition and stochastic partial air flow and air pressure, In_2O_3 covered the SnO_2 nanochains unevenly. So there exists a different thickness in a nano-core–shell structure, and even some places are bare core because of not being covered.

The PL spectra of SnO_2/In_2O_3 1D nano-core–shell structures at room temperature were measured by using a xenon lamp as an excitation source, which is shown in Fig. 4. It is clear that there are three strong peaks at 397, 451, and 468 nm, respectively. Also two weak peaks are observed at 483 and 492 nm. Besides, two shoulder peaks at 353 and 511 nm are also found in the PL spectrum. It has been observed that PL peak of In_2O_3 nanotubes and nanowires is at 475 and 450 nm, respectively, in previous reports [19–21]. The PL studies of SnO_2 nanostructures, PL peaks at 392, 439, and 399 nm have also been reported [16,19]. Clearly, the PL spectra that we have received have some difference from previous reports. The emissions at these peaks are obviously not the band-to-band transition because of the wide band gap of bulk SnO_2 and In_2O_3 [19]. The outer electronic structures of In and Sn are $4d^{10}5s^25p^1$, and $4d^{10}5s^25p^2$, respectively. Hence, the ability of the oxygen atom to comkbine with both Sn and In atoms is nearly the same for approximate outer electronic structures. The uninterrupted contention of the oxygen atom easily leads to the formation of oxygen vacancies and electronic defaults on the interface. In addition, the mismatch of two lattices of SnO_2 and In_2O_3 may also cause some faults. Therefore, the present PL emissions may be attributed to other luminescence centres,

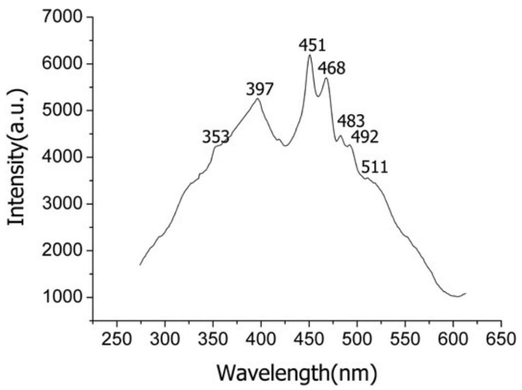

Fig. 4. Room temperature PL spectra of the SnO_2/In_2O_3 1D nano-core–shell structures.

such as oxygen vacancies, defects in the interface between the In_2O_3 and SnO_2.

4. Conclusion

In summary, SnO_2/In_2O_3 1D nano-core–shell structures have been synthesized at 1350 °C by thermal evaporation of the mixture of metal Sn, $Fe(NO_3)_3$ powders and In particles. EDX, SAED and HREM have been jointly applied to phase identification and microstructure characterization in this 1D nanostructure. The characteristic orientation relationship of core and shell was educed from microstructure analysis, $[001]_{In_2O_3} \parallel [001]_{SnO_2}$, $(010)_{In_2O_3} \parallel (010)_{SnO_2}$. Owing to the different melting and evaporation speed resulting from the different existence state of indium and tin reagent, 1D nano-core–shell structures are formed. The photoluminescence properties have some distinctness from previous works, which may be related to interface structures between the indium oxide and tin oxide.

Acknowledgements

This work is supported by the National Outstanding Young Scientist Foundation for X.L. Ma (Grant No. 50325101) and the Special Funds for the Major State Basic Research Projects of China (Grant No. 2002CB613503). Master X.G. Liu and J.M. Liang are also acknowledged for the help to measure the PL spectra.

References

[1] A.M. Morales, C.M. Lieber, Science 279 (1998) 208.
[2] M.H. Huang, S. Mao, H. Feick, H.Q. Yan, Y.Y. Wu, H. Kind, E. Weber, R. Russo, P.D. Yang, Science 292 (2001) 1897.
[3] Z.W. Pan, Z.R. Dai, Z.L. Wang, Science 291 (2001) 1947.
[4] Y. Zhang, K. Suenaga, C. Colliex, S. Iijima, Science 81 (1998) 973.
[5] Y. Xie, Z.P. Qiao, M. Chen, X.M. Liu, Y.T. Qian, Adv. Mater. 11 (1999) 1512.
[6] X.C. Wu, W.H. Song, B. Zhao, W.D. Huang, M.H. Pu, Y.P. Sun, J.J. Du, Solid State Commun. 115 (2000) 683.
[7] Q. Li, C.R. Wang, Appl. Phys. Lett. 82 (2003) 1398.
[8] J.Q. Hu, Y. Bando, Z.W. Liu, T. Sekiguchi, D. Golberg, J.H. Zhan, J. Amer. Chem. Soc. 125 (2003) 11306.
[9] J.Q. Hu, X.M. Meng, Y. Jiang, C.S. Lee, S.T. Lee, Adv. Mater. 15 (2003) 70.
[10] H.Z. Zhang, X.H. Luo, J. Xu, B. Xiang, D.P. Yu, J. Phys. Chem. B 108 (2004) 14866.
[11] T.A. Crowley, B. Daly, M.A. Morris, D. Erts, O. Kazakova, J.J. Boland, B. Wu, J.D. Holmes, J. Mater. Chem. 15 (2005) 2408.
[12] M. Law, H. Kind, B. Messer, F. Kim, P.D. Yang, Angew. Chem. Int. Ed. 41 (2002) 2405.
[13] C. Li, D.H. Zhang, S. Han, X.L. Liu, T. Tang, C.W. Zhu, Adv. Mater. 15 (2003) 143.
[14] P. Nguyen, H.T. Ng, T. Yamada, M.K. Smith, J. Li, J. Han, M. Meyyappan, Nano Lett. 4 (2004) 651.
[15] Z.R. Dai, Z.W. Pan, Z.L. Wang, Solid State Commun. 118 (2001) 351.
[16] J.Q. Hu, X.L. Ma, N.G. Shang, Z.Y. Xie, N.B. Wang, C.S. Lee, S.T. Lee, J. Phys. Chem. B 106 (2002) 3823.
[17] J.Y. Lao, J.Y. Huang, D.Z. Wang, Z.F. Ren, Adv. Mater. 16 (2004) 65.
[18] Y.B. Li, Y. Bando, D. Golberg, Adv. Mater. 16 (2004) 581.
[19] J.X. Wang, H.Y. Chen, Y. Gao, D.F. Liu, L. Song, Z.X. Zhang, X.W. Zhao, X.Y. Dou, S.D. Luo, W.Y. Zhou, G. Wang, S.S. Xie, J. Cryst. Growth 284 (2005) 73.
[20] J.S. Jeong, J.Y. Lee, C.J. Lee, S.J. An, G.C. Yi, Chem. Phys. Lett. 384 (2004) 246.
[21] X.P. Shen, H.J. Liu, X. Fan, Y. Jiang, J.M. Hong, Z. Xu, J. Cryst. Growth 276 (2005) 471.